analytical chemistry

pubs.acs.org/ac

Article

Rheology of the Electric Double Layer in Electrolyte Solutions

Riccardo Funari,[§] Atsushi Matsumoto,[§] John R. de Bruyn, and Amy Q. Shen*

Cite This: *Anal. Chem.* 2020, 92, 8244−8253

Read Online

ACCESS | Metrics & More | Article Recommendations | Supporting Information

ABSTRACT: Electric double layers (EDLs) are ionic structures formed on charged surfaces and play an important role in various biological and industrial processes. An extensive study in the past decade has revealed the structure of the EDL in concentrated electrolyte solutions of both ordinary salts and ionic liquids. However, how the EDL structure affects their material properties remains a challenging topic due to technical difficulties of these measurements at nanoscale. In this work, we report the first detailed characterization of the viscoelasticity of the EDL formed over a wide range of ion concentrations, including concentrated electrolyte solutions. Specifically, we investigate the complex shear modulus of the EDL by measuring the resonant frequency and the energy dissipation of a quartz crystal microbalance (QCM), a surface-sensitive device, immersed in aqueous solutions containing three types of solutes: an ionic liquid, 1-butyl-3-methylimidazolium chloride (BmimCl); an ordinary salt, sodium chloride (NaCl); and a nonelectrolyte, ethylene glycol (EG). For the two electrolyte solutions, we observe a monotonic decrease in the resonant frequency and a monotonic increase in the energy dissipation with increasing ion concentrations due to the presence of the EDL. The complex shear modulus of the EDL is estimated through a wave propagation model in which the density and shear modulus of the EDL decay exponentially toward those of the bulk solution. Our results show that both the storage and the loss modulus of the EDL increase rapidly with increasing ion concentrations in the low ion concentration regime (<1 M) but reach saturation values with similar magnitude at a sufficiently high ion concentration. The shear viscosity of the EDL near the charged QCM surface is approximately 50 times for NaCl solutions and 500 times for BmimCl solutions of the bulk solution value at the saturation concentration. We also demonstrate that QCM can be utilized for analyzing the rheological properties of the EDL, thus providing a complementary, low-cost, and portable alternative to conventional laboratory instruments such as the surface force apparatus. Our results elucidate new perspectives on the viscoelastic properties of the EDL and can potentially guide device optimization for applications such as biosensing and fast charging of batteries.

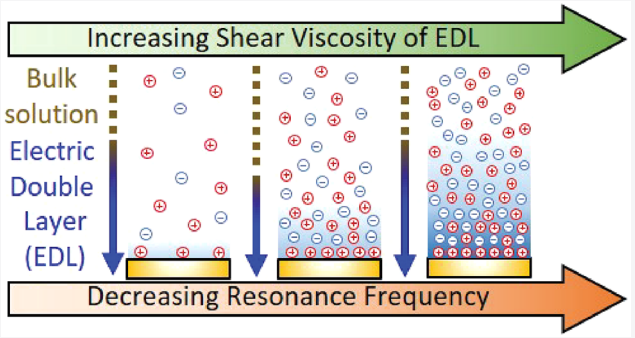

When a charged surface is immersed in an electrolyte solution, dissolved ions are assembled on it, and an electric double layer (EDL) is formed at the solid−liquid interface to screen the charge of the surface.[1−5] The EDL therefore plays a crucial role in various biological and industrial processes, such as biosensing,[6−8] enzymology,[9−11] coatings,[12,13] and storing energy in batteries.[5,14−16] The electrostatic screening mechanism[1] and the resulting properties, such as double layer capacitance[17] and shear viscosity,[18] of the EDL are well understood at low ion concentrations. On the other hand, today's ever-growing activities in biotechnology and new energy development have led to an increasing need for understanding the EDL behavior in concentrated electrolyte solutions, such as ionic liquids (ILs).[19] Accordingly, an extensive study has been conducted in the past decade to understand the structure of the EDL in concentrated electrolyte solutions, reporting an unexpected screening behavior in which the screening length increased with increasing ion concentrations at high ion concentration regime, in contrast with the trend predicted by the Debye−Hückel (DH) theory for dilute electrolyte solutions (see more details below).[20−38] However, how the structure of the EDL affects their rheological properties remains a challenging topic due to technical difficulties of measuring the mechanical properties at nanoscale. Better understanding of the dynamics of the EDL will guide device optimization for applications in biosensors and fast charging of batteries.

The surface force apparatus (SFA) evaluates the properties of materials confined at the nanoscale.[21] SFA has been a useful tool for measuring the rheological properties of the EDL.[39−41] For example, Kurihara and co-workers[39,40] utilized a SFA equipped with a resonance shear system to investigate the shear viscosity of ILs confined between two charged silica

Received: February 3, 2020
Accepted: May 18, 2020
Published: May 18, 2020

https://dx.doi.org/10.1021/acs.analchem.0c00475
Anal. Chem. 2020, 92, 8244−8253

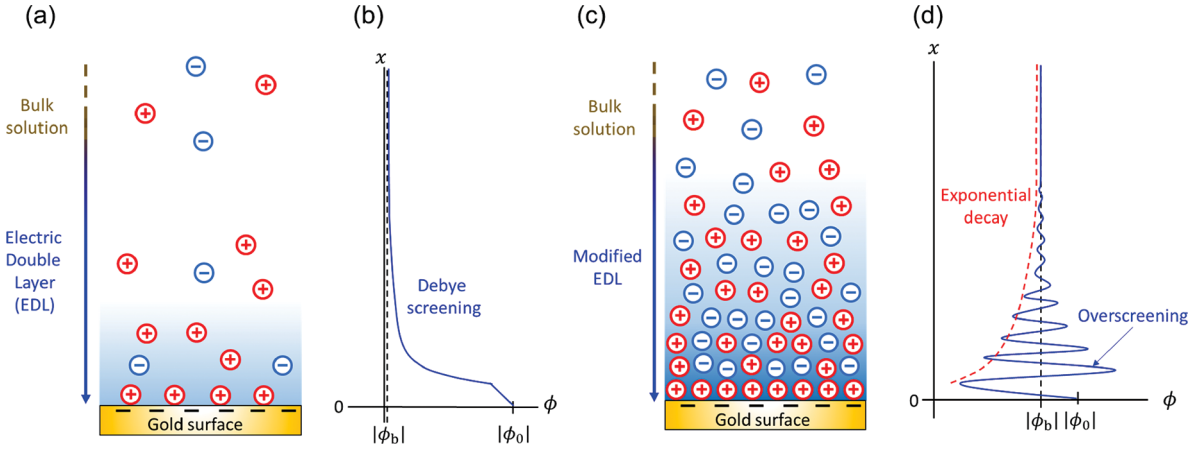

Figure 1. Schematic illustration of an electric double layer (EDL) formed on a gold coated quartz crystal having an electric potential ϕ_0, with the corresponding electric potential ϕ − distance x profile. (a) The Gouy−Chapman-Stern (GCS) model[1] based on the Debye−Hückel theory[52] is applied for solutions at low ion concentrations. The EDL consists of the cation-rich layers. (b) The value of electric potential ϕ initially decreases due to cations assembled over the negatively charged interface, followed by the exponential decay of ϕ to the electric potential of the bulk solution (ϕ_b) due to the Debye screening. (c) According to Gavish et al.,[31] an EDL at high ion concentration consists of a multilayered ionic structure. (d) The value of electric potential ϕ decreases significantly due to the overscreening caused by excess cations assembled over the surface, followed by the exponential decay of the oscillatory electric potential to ϕ_b (red dashed line). In these schematics, cations and anions are represented as red plus circles and blue minus circles, respectively. Different shades of blue color in the background represent the area with different density and viscosity values from those of the bulk solution. Note that we do not distinguish associated and dissociated ion pairs in the schematics.

surfaces. They showed that the shear viscosity of the ILs near the silica surface was 1−3 orders of magnitude larger than that of the bulk ILs. This confinement-enhanced shear viscosity is observed not only for ILs but also for aqueous[42] and some oil-based solutions.[43] Thus, the EDL might not be completely responsible for the enhanced shear viscosity of confined ILs observed by the SFA. In order to evaluate the shear modulus of the EDL, measurements need to be performed using an independent technique.

The quartz crystal microbalance (QCM) is a surface-sensitive device which has been used to measure the rheological properties of materials, such as polymeric nano-layers[44] and biofilms.[45] The QCM is based on an AT-cut quartz crystal with metal electrodes (usually gold) deposited on its surfaces. Shear waves are excited in the quartz crystal by applying an oscillating voltage across the electrodes, and the resonant frequency of the system is reduced by the mass and viscoelasticity of materials deposited or adsorbed onto the crystal surface.[46,47] Several research groups[18,48−50] have studied the QCM response for dilute electrolyte solutions, showing a shift of the resonant frequency due to the presence of EDL formed on the QCM gold surface. Combining QCM with impedance analysis,[51] Etchenique and Buhse[18] reported that the loss modulus of an EDL in dilute solutions of sodium chloride was always larger than its storage modulus, and that while the loss modulus increased with the increasing ion concentration, the storage modulus remained constant following a steep increase at low ion concentrations (<10 mM). Their studies did not cover the behavior in concentrated electrolyte solutions. These results motivated us to employ QCM to investigate the rheological properties of the EDL in more concentrated electrolyte solutions.

In this work, we report the first characterization of the complex shear modulus of the EDL over a wide range of ion concentrations by measuring the resonant frequency and the energy dissipation of a QCM gold-coated quartz oscillator. We investigate aqueous solutions containing three types of solutes: an ionic liquid, 1-butyl-3-methylimidazolium chloride (BmimCl); an ordinary salt, sodium chloride (NaCl); and a nonelectrolyte, ethylene glycol (EG). For the two electrolyte solutions, we observe a monotonic decrease in the resonant frequency and a monotonic increase in the energy dissipation with the increasing ion concentration due to the presence of EDL. The complex shear modulus of the EDL is estimated using a wave propagation model in which the density and shear modulus of the EDL decay exponentially toward those of the bulk solution. Our results show that the EDL's shear modulus increases with increasing ion concentrations, and the shear viscosity near the charged QCM surface is approximately 2 orders of magnitude larger than that of the bulk solution, consistent with the results reported from the surface force apparatus. Our results demonstrate that the QCM can be utilized for analyzing the viscoelasticity of the EDL in electrolyte solutions, thus providing a complementary, low cost and portable alternative to conventional laboratory instruments such as the surface force apparatus.

EDL STRUCTURES AND THE SCREENING LENGTH

In this section, we summarize the structure of the EDL and the current understanding of the screening length in electrolyte solutions in the low- and high-concentration regimes, based on the literature. Figure 1(a) shows a schematic of an EDL formed on a negatively charged surface immersed in a dilute electrolyte solution. The interaction between the gold substrate and electrolytes has been measured by atomic force microscopy,[20,22,53] showing that even without applying a voltage to the gold surface, the electrolytes form an EDL on the gold surface and the thickness of the innermost ionic layer is compatible with the size of the cations (similar evidence is reported in Section S4 in the Supporting Information). According to the Gouy−Chapman-Stern (GCS) model,[1] a layer of cations is formed on the negatively charged surface to partially decrease the electric potential in the solution. A cation-rich layer is formed over the cation layer to screen the residual electric potential, which decreases exponentially with distance as predicted by the Debye−Hückel (DH) theory

https://dx.doi.org/10.1021/acs.analchem.0c00475
Anal. Chem. 2020, 92, 8244−8253

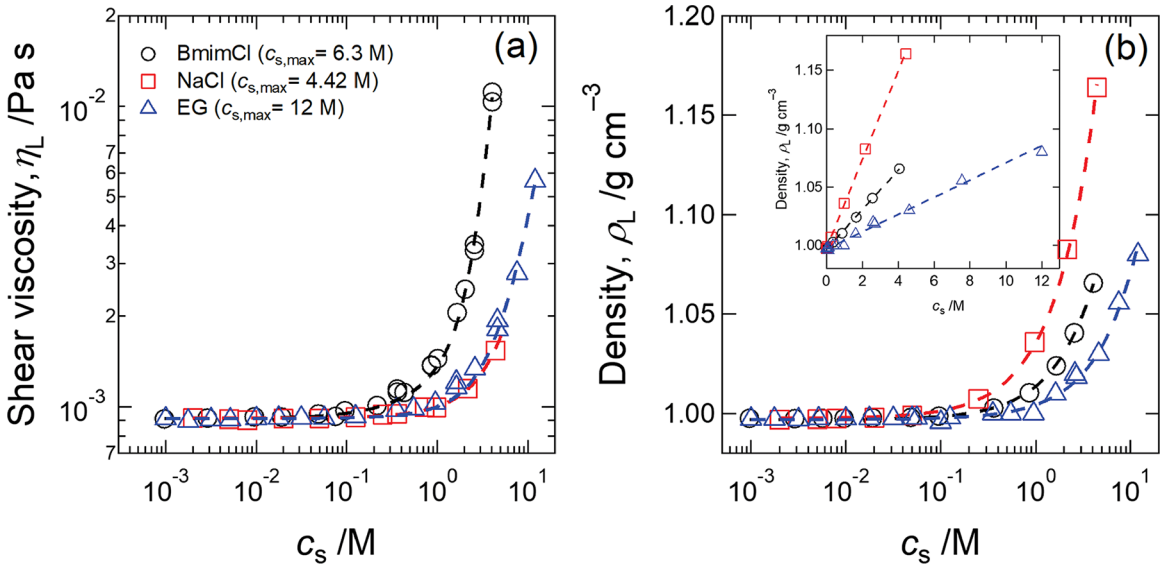

Figure 2. (a) The shear viscosity η_L at 25 °C is plotted as a function of the concentration of BmimCl (black circles), NaCl (red squares), and EG (blue triangles). The measured η_L is fitted with a polynomial function (eq 4, dashed curves). (b) The density ρ_L at room temperature (25 ± 1 °C) is plotted as a function of the concentration of BmimCl (black circles), NaCl (red squares), and EG (blue triangles). The measured ρ_L is fitted with the linear function (eq 5, dashed curves). The inset highlights the linear relationship between the density and concentration of the analytes.

(Figure 1(b)).[52] The characteristic decay length of the electric potential is referred to as the screening length. However, recent experimental[20−24,26−30,32,35,53,54] and theoretical[25,31,33,34,36,37,55−59] studies have shown that the electrostatic screening mechanism in concentrated electrolyte solutions is significantly different from that in dilute electrolyte solutions.

Figure 1(c) shows a schematic of a modified EDL formed on a negatively charged surface immersed in a concentrated electrolyte solution, with the ion distribution depicted on the basis of the electric potential profile, shown in Figure 1(d), predicted by Gavish et al.[31] Similar to the GCS model, a cation layer is formed over the negatively charged surface. In this case, however, the charge in the cation layer overcompensates the charge of the surface, leading to the formation of an anion-rich layer over the cation layer. This anion-rich layer again overcompensates the positive charge of the cation layer. This phenomenon, in which charges in a layer are overcompensated by charges in the next layer, is called *overscreening*.[60] The overcompensation damps as the distance from the surface increases, and the electric potential decays to that of the bulk solution. The damping of the electric potential oscillation at high ion concentrations is caused by the strong ionic correlations occurring in concentrated electrolyte solutions. As a result, a multilayered ionic structure with oscillating charge density that decays over distance to that of the bulk solution is formed in concentrated electrolyte solutions. The oscillation of the electric potential decays exponentially, as shown by the red dashed line in Figure 1(d), and the characteristic decay length of this oscillation is considered as the screening length.[31]

Smith et al.[30] investigated the screening length λ_D in solutions of sodium chloride and an IL from low to high concentrations. They showed that λ_D decreased with increasing ion concentrations in the low-concentration regime, consistent with the DH theory. However, as the concentration was further increased, λ_D reached a minimum and then increased again. The increase of λ_D over increasing c_s in the high-concentration regime is caused by strong ionic correlations present at high c_s.[34] With a series of experiments, Lee et al.[56] found that regardless of the type of electrolytes, the value of λ_D followed a universal relationship with respect to the Debye screening length λ_{Debye} and the ion diameter a,

$$\lambda_D = \lambda_{Debye} \text{ for } \lambda_{Debye} \geq a \tag{1}$$

$$\lambda_D \sim \lambda_{Debye}\left(\frac{a}{\lambda_{Debye}}\right)^3 \text{ for } \lambda_{Debye} < a \tag{2}$$

where

$$\lambda_{Debye} = \sqrt{\frac{\varepsilon_r \varepsilon_0 k_B T}{2000 c_s N_A e^2}} \tag{3}$$

Here ε_r, ε_0, k_B, T, N_A, and e are the dielectric constant of the mixture, the dielectric constant, the Boltzmann constant, the absolute temperature, the Avogadro constant, and the elementary charge. The breakdown of the DH theory is predicted to occur when $\lambda_{Debye} \approx a$.[56]

EXPERIMENTAL METHODS

Materials. 1-Butyl-3-methylimidazolium chloride (BmimCl) (purity >99%) was purchased from Ionic Liquid Technologies, Germany. Ethylene glycol (EG) was purchased from Sigma-Aldrich, Japan. Sodium chloride (NaCl) was purchased from Wako Pure Chemicals, Japan. All chemicals were used as received. Milli-Q water that had passed through a Q-POD Element unit (Millipore) and had a resistivity higher than 18.2 MΩ cm was used as a solvent.

Preparation of the Test Solutions. High-concentration solutions were prepared by directly adding the components into a glass vial, while low-concentration solutions were prepared by diluting more concentrated solutions. Since BmimCl is highly hygroscopic, it was stored and handled in a glovebox under an argon atmosphere. The analyte concentration, c_s, was calculated as $c_s = m_s\rho_L/M_0 m_{tot}$, where ρ_L is the density of the bulk solution, M_0 is the molar mass of

https://dx.doi.org/10.1021/acs.analchem.0c00475
Anal. Chem. 2020, 92, 8244−8253

analyte, m_s is the mass of analyte, and m_{tot} is the solution mass. The concentrations of pure BmimCl, pure EG, and the saturation concentration of NaCl (i.e., $c_{s,max}$) in our experimental conditions are 6.3, 12, and 4.42 M, respectively.

Shear Viscosity Measurements. The shear viscosity of the solution at shear rates ranging from 50 to 10,000 s^{-1} was measured using a microfluidic slit rheometer (m-VROC, RheoSense Inc.). We employed a straight rectangular channel 50 μm in height, 3.0 mm in width, and 8.8 mm in length. The temperature was set at 25 °C and controlled by a Peltier system. The measurement principle is provided elsewhere.[61] The measured shear viscosity was independent of the shear rate over the measured shear rate range, and the shear viscosity of the bulk solution η_L was determined by averaging over shear rates measured. Figure 2(a) shows the dependence of η_L on c_s for solutions of BmimCl, NaCl, and EG. η_L increased monotonically with increasing c_s. We fitted the measured η_L as a function of the analyte concentration using an empirical polynomial function

$$\eta_L = \eta_{water}(1 + Ac_s + Bc_s^2 + Dc_s^{3.5}) \quad (4)$$

where η_{water} = 0.912 mPa s is the shear viscosity of water at 25 °C. The best fits are shown as dashed curves in Figure 2(a), and the values of the corresponding fitting coefficients are given in Table 1. We confirmed that our bulk solutions exhibited Newtonian behavior up to 100 MHz (see more details in Section S1 of the Supporting Information).

Table 1. Fitting Coefficients Providing the Best Fit to the Empirical Polynomial Function for Shear Viscosity and Density of BmimCl, NaCl, and EG Solutions

solute	A (10^{-2} M^{-1})	B (10^{-3} M^{-2})	D (10^{-3} M^{-3})	E (10^{-2} M^{-1})
BmimCl	4.3 ± 0.8	0	6.8 ± 0.3	1.70 ± 0.02
NaCl	0.7 ± 0.1	2.0 ± 0.2	0	3.80 ± 0.03
EG	0.7 ± 0.1	3.1 ± 0.1	0	0.74 ± 0.01

Density Measurements. The density of the bulk solution ρ_L was measured by using a density meter (DMA 35 Basic, Anton Paar) at room temperature (25 ± 1 °C). Figure 2(b) shows the dependence of ρ_L on c_s for BmimCl, NaCl, and EG solutions. The density increased monotonically with increasing c_s. We fitted the measured ρ_L as a function of the analyte concentration using a linear function

$$\rho_L = \rho_{water}(1 + Ec_s) \quad (5)$$

where ρ_{water} = 0.997 g cm^{-3} is the density of water at 25 °C. The best fits are shown as dashed curves in Figure 2(b), and the values of the corresponding fitting coefficient are given in Table S1 of the Supporting Information.

Quartz Crystal Microbalance Measurements. The QCM device employed was an openQCM Q-1 (Novaetech, Italy) equipped with AT-CUT quartz sensors (I.E.V., Italy) with a resonant frequency of 10 MHz. The QCM device applies an oscillating potential of 0.7 V amplitude (offset 0 V) to the quartz sensor, and its resonance frequency and energy dissipation are recorded by a computer program provided by the manufacturer. The QCM sensors were cleaned before use by sonication in acetone, isopropyl alcohol, and Milli-Q water for 5 min. The sample solutions were contained in a polymethylmethacrylate (PMMA) cell open to the gold surface of the QCM. As shown in Figure 3(a), the cell was initially filled with 200 μL of Milli-Q water. After the quartz resonant frequency had stabilized, 20 or 50 μL of water was removed from the cell and replaced with an equal volume of concentrated analyte solution to increase the analyte concentration. The QCM frequency was allowed to restabilize, and then the procedure was repeated. In this way, multiple concentrations of analyte could be tested in a single experiment on the same sensor, performed over a period of up to 15 h. Our measurements covered c_s values ranging from 0 to 3.45, 3.60, and 3.95 M for BmimCl, NaCl, and EG solutions, respectively. All measurements were done using the first harmonic of the crystal (n = 1). An example of the data obtained from this experimental protocol is shown in Figure 3(b), in which the variation in the QCM frequency shift Δf_{exp} and energy dissipation shift ΔD_{exp} with BmimCl concentration is evident. In this figure, we chose the resonant frequency and dissipation at c_s = 0 M, corresponding to pure water, as the reference signals, so $\Delta f_{exp} = f(c_s) - f(0)$ and $\Delta D_{exp} = D(c_s) - D(0)$, respectively. The QCM resonance was altered by the injection of the concentrated BmimCl sample, resulting in a sudden drop in the resonant frequency. The quartz sensor then stabilized over time, with the stabilization time depending on c_s. The opposite behavior was observed for the dissipation signal, with a sudden increase in the energy dissipation when introducing the concentrated BmimCl sample. Figure 3(b) shows that, as the concentration of BmimCl increases, the value of Δf_{exp} becomes more negative, while ΔD_{exp} progressively increases. Similar profiles of the QCM frequency and dissipation shifts were observed for NaCl and EG solutions. Measurements were performed in triplicate to allow an estimation of the standard deviation at each concentration.

Although Δf_{exp} is negative, we plot its absolute value $|\Delta f_{exp}|$ for simplicity to highlight the change in the frequency shift due to the mass and viscoelastic effects of substances adsorbed on the QCM sensor.

WAVE PROPAGATION MODEL

In order to evaluate the complex shear modulus of the EDL, we now consider how the EDL is detected by the QCM. Here, we consider a three-dimensional Cartesian coordinate system (x, y, z) where x is the distance from the quartz surface, as shown in Figure 1. Thus, x = 0 represents the position of the charged gold QCM surface, while $x = \infty$ is far from the surface in the bulk solution. We assume that the concentration and density of the EDL depend only on the distance x from the surface, so that the rheological properties are independent of y and z.

QCM frequency and dissipation shifts due to the EDL can be observed when its density ρ_D and complex shear modulus $G^*(= G' + iG'')$, where G' and G'' are storage and loss moduli) are different from those of the bulk solution. This happens when the concentration of either cations or anions in the EDL is different from that of the bulk solution. Here, we assume that the magnitude of the density and the complex modulus of the EDL decays exponentially with x toward those of the bulk solution in the low- and high-concentration regimes, which can be expressed by[18,39]

$$\rho_D = \rho_L + (\rho_{D,max} - \rho_L)\exp\left(-\frac{x}{\lambda_D}\right) \quad (6)$$

https://dx.doi.org/10.1021/acs.analchem.0c00475
Anal. Chem. 2020, 92, 8244−8253

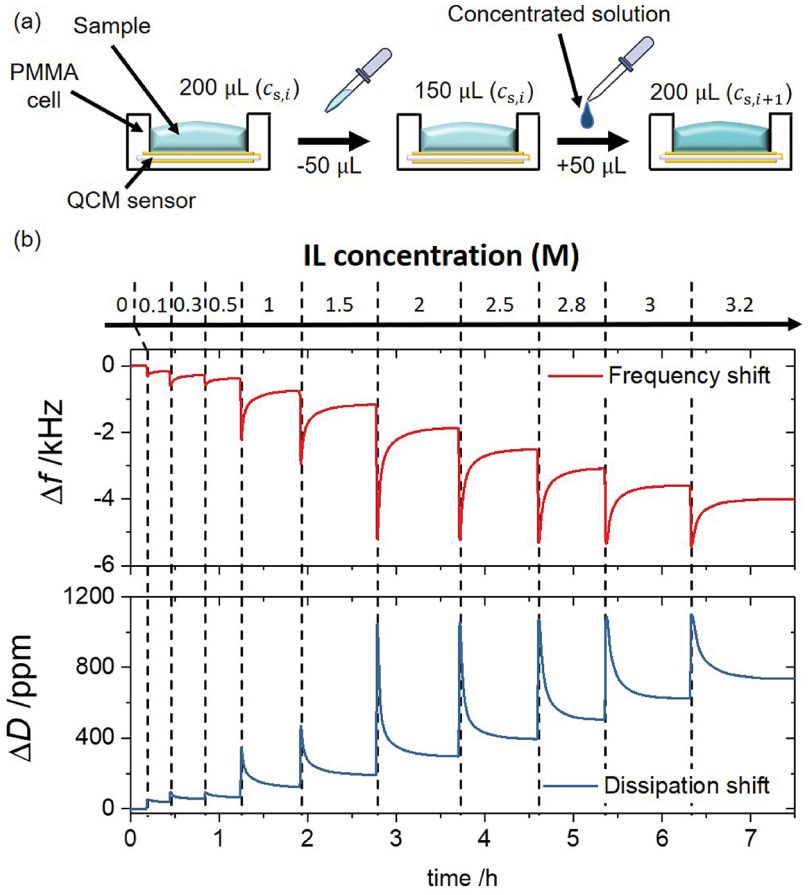

Figure 3. (a) Analyte concentration is adjusted by replacing the previous solution with an equal volume of concentrated analyte solution. In the schematic, 50 μL of the previous solution at $c_{s,i}$ is replaced with 50 μL of concentrated solution to increase the concentration to be $c_{s,i+1}$. (b) QCM frequency shift Δf_{exp} (red curve) and dissipation shift ΔD_{exp} (blue curve) over the course of a series of measurements as the concentration of BmimCl is increased from 0 to ≈3 M. The resonant frequency and dissipation at c_s = 0 M (corresponding to pure water) are chosen as the reference signals, thus $\Delta f_{exp} = f(c_s) - f(0)$ and $\Delta D_{exp} = D(c_s) - D(0)$, respectively. The changes in the ion concentration (indicated by the vertical dashed lines) lead to a sudden perturbation in both quartz resonant frequency and energy dissipation, followed by the subsequent stabilization over time. The next concentration is tested only when the QCM signals have reached equilibrium state and become steady.

$$G'_D = G'_{D,max} \exp\left(-\frac{x}{\lambda_D}\right) \tag{7}$$

$$G''_D = G''_L + (G''_{D,max} - G''_L) \exp\left(-\frac{x}{\lambda_D}\right) \tag{8}$$

where $\rho_{D,max}$, $G'_{D,max}$, and $G''_{D,max}$ are the limiting values of density and storage and loss moduli of the EDL as x approaches zero. The characteristic length of the exponential decay for ρ_D, G'_D, and G''_D in both low- and high-ion-concentration regimes is denoted by the screening length λ_D, given by eqs 1 and 2. For electrolyte solutions, it is reasonable to assume $\rho_{D,max}$ to be the density at the saturation concentration, since the concentration of ions is much larger at $x = 0$ than at $x = \infty$. In fact, Etchenique and Buhse[18] showed that $\rho_{D,max}$ for sodium chloride solutions increased with increasing concentration, asymptotically approaching its saturation density at concentrations larger than 20 mM.

A wave propagation model proposed by Voinova et al.[62] predicts the frequency shift Δf_{exp} and the dissipation shift ΔD_{exp} of a quartz crystal covered by viscoelastic layers below a semi-infinite Newtonian fluid. For an EDL with x-dependent properties, Voinova's model yields

$$\Delta f_{exp} = \Delta f_B + \Delta f_{EDL} \tag{9}$$

$$\Delta D_{exp} = \Delta D_B + \Delta D_{EDL} \tag{10}$$

where the contribution of the bulk solution, denoted by the subscript B, and the EDL are given by

$$\Delta f_B = -n^{1/2} f_F^{3/2} \sqrt{\frac{\eta_L \rho_L}{\pi \rho_q G_q}} \tag{11}$$

$$\Delta f_{EDL} = -\frac{2nf_F^2}{\sqrt{G_q \rho_q}} \rho_L \int_0^\infty \left(\frac{\rho_D}{\rho_L} - \eta_L \frac{\omega G''_D}{G'^2_D + G''^2_D}\right) dx \tag{12}$$

$$\Delta D_B = 2n^{-1/2} f_F^{1/2} \sqrt{\frac{\eta_L \rho_L}{\pi \rho_q G_q}} \tag{13}$$

$$\Delta D_{EDL} = \frac{4f_F}{\sqrt{G_q \rho_q}} \rho_L \eta_L \int_0^\infty \frac{\omega G'_D}{G'^2_D + G''^2_D} dx \tag{14}$$

Note that ρ_D, G'_D, and G''_D are functions of x as given by eqs 6, 7, and 8. Here n is an odd integer indicating the harmonic number, f_F is the fundamental resonant frequency of the bare

https://dx.doi.org/10.1021/acs.analchem.0c00475
Anal. Chem. 2020, 92, 8244−8253

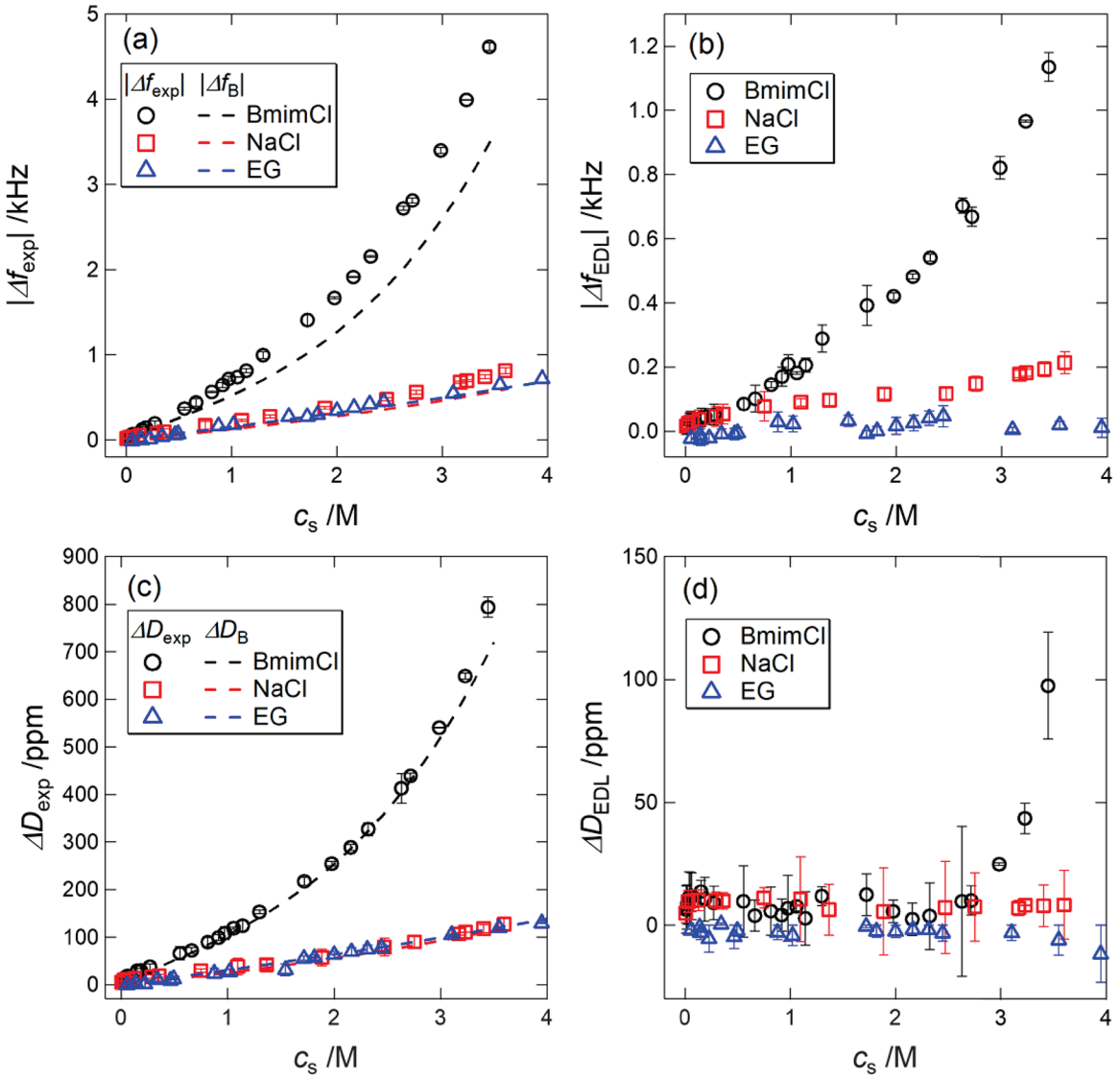

Figure 4. (a) The absolute value of the QCM frequency shift at steady state $|\Delta f_{exp}|$ is plotted as a function of the concentration of BmimCl (black circles), NaCl (red squares), and EG (blue triangles). The dashed curves are the frequency shifts $|\Delta f_B|$ due to the bulk solution, obtained by fitting the estimated $|\Delta f_B|$ predicted by eq 11 with a polynomial function (see Figure S7 of the Supporting Information). (b) Frequency shift by the EDL, $|\Delta f_{EDL}| = \Delta f_{exp} - \Delta f_B|$, is plotted as a function of the concentration of BmimCl (black circles), NaCl (red squares), and EG (blue triangles). (c) The value of the QCM dissipation shift at steady state ΔD_{exp} is plotted as a function of the concentration of BmimCl (black circles), NaCl (red squares), and EG (blue triangles) solutions. The dissipation shifts ΔD_B due to the bulk solution are represented by the dashed curves, estimated from the fit of the predicted ΔD_B by eq 13 to a polynomial function. (d) Dissipation shift by the EDL, $\Delta D_{EDL} = \Delta D_{exp} - \Delta D_B$, is plotted as a function of the concentration of BmimCl (black circles), NaCl (red squares), and EG (blue triangles) solutions.

quartz crystal, and $\rho_q = 2.648$ g cm^{-3} and $G_q = 2.947 \times 10^{11}$ g cm^{-1} s^{-2} are the density and the storage shear modulus of the AT-cut quartz crystal, respectively. Consequently, the storage G'_D and loss G''_D moduli of the EDL (eqs 7 and 8) can be estimated based on the value of Δf_{EDL} and ΔD_{EDL} being extracted from our QCM based measurements.

RESULTS AND DISCUSSION

Frequency/Dissipation Shifts. Figure 4(a) shows the absolute value of the frequency shift $|\Delta f_{exp}|$ as a function of c_s for solutions of BmimCl, NaCl, and EG. The value of $|\Delta f_{exp}|$ at each concentration was estimated from the frequency shift at steady state after the quartz resonator was stabilized. $|\Delta f_{exp}|$ increased monotonically with increasing c_s for all three analytes. The frequency shift $|\Delta f_B|$ due to the bulk solution was calculated from eq 11 using the shear viscosity and density data presented in Figure 2. The dashed curves in Figure 4(a) were obtained by fitting $|\Delta f_B|$ with a polynomial function of c_s (see Figure S5 of the Supporting Information).

The measured values of $|\Delta f_{exp}|$ for the nonelectrolyte EG solutions are well described by eq 11. On the other hand, the frequency shifts measured for both BmimCl and NaCl were substantially larger than the values predicted by eq 11. Since both BmimCl and NaCl solutions consist of water and dissolved ions, it is reasonable to attribute the observed excess frequency shift to the presence of an EDL. The frequency shift caused by the EDL, $|\Delta f_{EDL}|$, was estimated by subtracting $|\Delta f_B|$ from $|\Delta f_{exp}|$. Figure 4(b) shows the dependence of $|\Delta f_{EDL}|$ on c_s for solutions of BmimCl, NaCl, and EG. As expected, the values of $|\Delta f_{EDL}|$ for EG solutions were close to zero over the measured c_s range. On the other hand, for BmimCl solutions,

https://dx.doi.org/10.1021/acs.analchem.0c00475
Anal. Chem. 2020, 92, 8244−8253

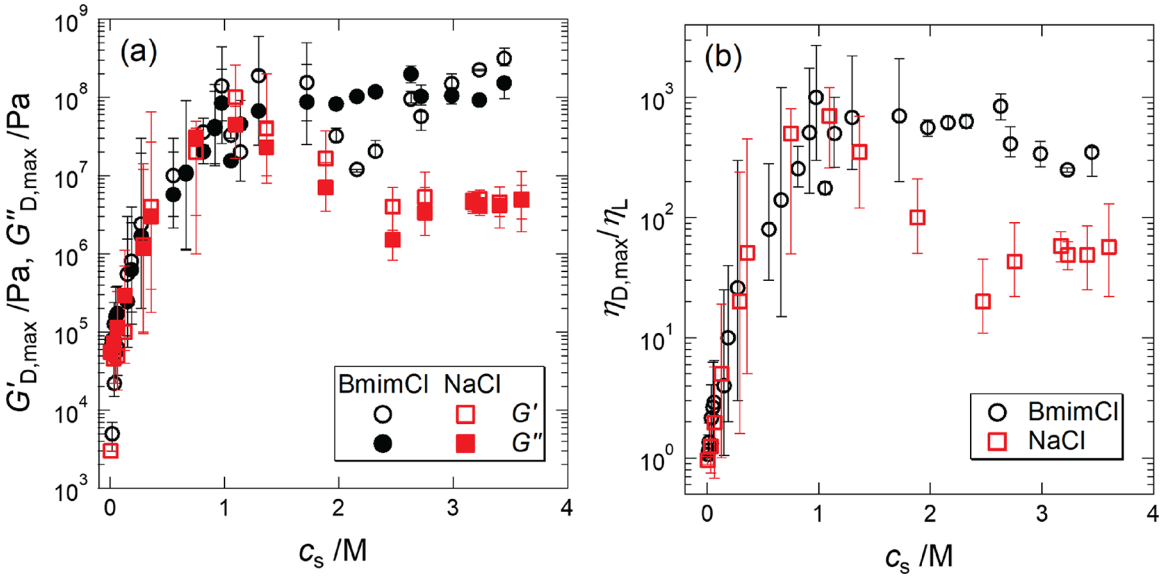

Figure 5. (a) The value of $G'_{D,max}$ and $G''_{D,max}$ (complex shear modulus at $x = 0$) is plotted as a function of the ion concentration c_s of BmimCl (black circles) and NaCl (red squares) solutions. Both $G'_{D,max}$ and $G''_{D,max}$ increase with increasing c_s for both solutions. (b) The ratio of $\eta_{D,max}$ (at $x = 0$) to η_L for BmimCl (black circles) and NaCl (red squares) solutions is plotted as a function of c_s. This ratio reaches a saturation value at high c_s of approximately 500 for BmimCl and 50 for NaCl solutions.

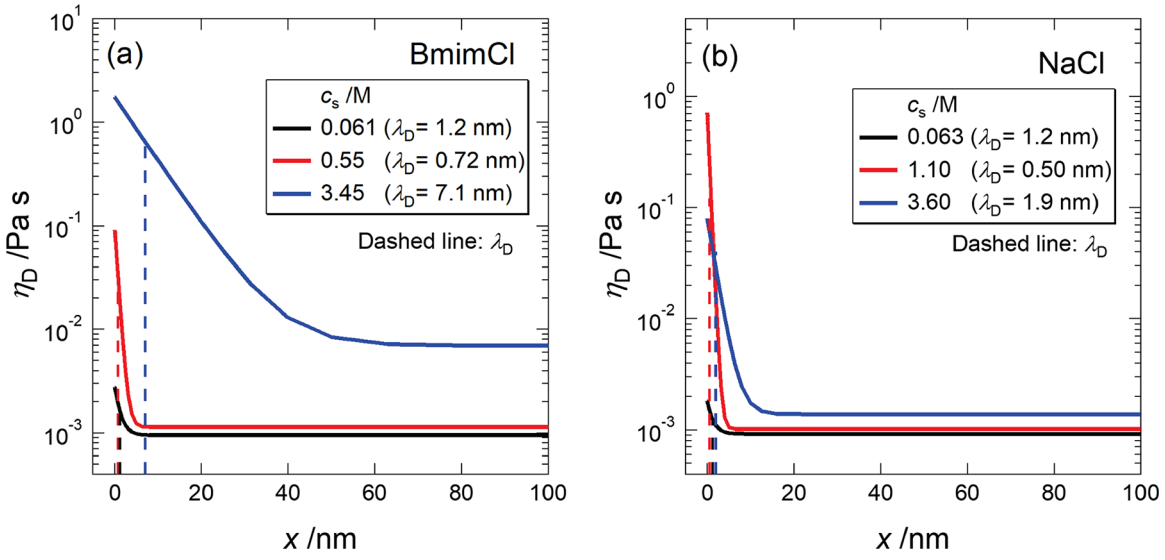

Figure 6. Based on eq 8, shear viscosity $\eta_D = G''_D/\omega$ of the EDL is plotted against the distance x from the quartz sensor surface at low (black solid curve), intermediate (red solid curve), and high (blue solid curve) ion concentrations c_s for (a) BmimCl and (b) NaCl solutions. The dashed lines indicate the screening length λ_D at each concentration.

the values of $|\Delta f_{EDL}|$ increased monotonically with increasing c_s. A similar trend was observed for NaCl solutions.

Figure 4(c) shows the value of the dissipation shift ΔD_{exp} as a function of c_s for solutions of BmimCl, NaCl, and EG. The value of ΔD_{exp} at each concentration was estimated from the dissipation shift at steady state when the quartz resonator was stabilized. Similarly, the values of the dissipation shift caused by the EDL, $\Delta D_{EDL} = \Delta D_{exp} - \Delta D_B$, were close to zero for EG solutions, while small excess dissipation shifts were observed for BmimCl and NaCl solutions over the measured c_s range. The values of ΔD_{EDL} for the BminCl solutions increased from 0 to about 10 ppm as c_s increased from 0 to 0.05 M and then remained as a constant up to c_s = 3 M. For c_s > 3 M, ΔD_{EDL} increased more significantly with increasing c_s. A similar trend was observed for NaCl solutions with reduced magnitude.

Complex Shear Modulus of the EDL. On the basis of the wave propagation model proposed above, the complex shear modulus of the EDL at $x = 0$ (i.e., $G'_{D,max}$ and $G''_{D,max}$) was determined by matching the frequency and dissipation shifts predicted by eqs 12 and 14 to the measured frequency $|\Delta f_{EDL}|$ and dissipation ΔD_{EDL} shifts. Here, $\rho_{D,max}$ = 1.08 g cm^{-3} is the density of pure BmimCl,[63] and $\rho_{D,max}$ = 1.25 g cm^{-3} is the density of the saturated NaCl solution.[64] The screening length λ_D in BmimCl solutions, shown in Figure S6 of the Supporting Information, was calculated based on the ion diameter a estimation using atomic force microscopy, while the dependence of ε_r on c_s was calculated using the effective medium theory in accordance with the method employed by Smith et al.[30] (see more details in Section S2 for dielectric constant and Section S3 for ion diameter in the Supporting Information).

https://dx.doi.org/10.1021/acs.analchem.0c00475
Anal. Chem. 2020, 92, 8244−8253

The dependence of λ_D on c_s for NaCl solutions has been reported in the literature.[30] Since the magnitude of experimental errors of the excess dissipation shift is similar to that of the ΔD_{EDL}, we envision a more sensitive QCM device incorporating a microfluidic cell to introduce the electrolytes continuously on the sensor surface can provide more accurate estimation of the complex modulus of the EDL in the future.

Figure 5(a) shows the dependence of $G'_{D,max}$ and $G''_{D,max}$ on c_s for BmimCl and NaCl solutions. For BmimCl solutions, both $G'_{D,max}$ and $G''_{D,max}$ increased rapidly with increasing c_s for $c_s < 1$ M, followed by a more gradual increase with further increase in c_s. The values of $G''_{D,max}$ were initially larger than $G'_{D,max}$ for $c_s <$ 0.1 M, but they became comparable at higher c_s. Similar behavior was observed for NaCl solutions. The estimated magnitude of $G'_{D,max}$ and $G''_{D,max}$ for NaCl at $c_s < 0.05$ M agreed well with the values reported in the literature.[18] We note that the apparent overshoot visible around 1 M for both solutions is likely an artifact due to large uncertainties in the resonant frequency of the QCM in the low c_s regime.

We also evaluated the difference between the limiting shear viscosity $\eta_{D,max} = G''_{D,max}/\omega$ of the EDL at $x = 0$ and the shear viscosity η_L of the bulk solution. The ratio of $\eta_{D,max}/\eta_L$ was plotted as a function of c_s in Figure 5(b). This ratio for BmimCl solutions increased rapidly with increasing c_s for $c_s < 1$ M and then reached a saturation value of ~500 at higher c_s, in good agreement with those reported for ILs estimated using SFA.[39] A similar trend was observed for NaCl solutions, with the ratio of $\eta_{D,max}/\eta_L$ reaching ~50 at higher c_s. We also observed that the concentration where $\eta_{D,max}$ started to level off was close to the concentration where $\lambda_{Debye} \sim a$ for both NaCl and BmimCl solutions. This result suggests that the structure of the EDL near the charged surface becomes independent of c_s for $c_s > 1$ M.

Figure 6 shows the shear viscosity $\eta_D = G''_D/\omega$ of the EDL versus distance x from the quartz sensor surface at low, intermediate, and high ion concentrations for BmimCl and NaCl solutions, calculated from eq 8. The shear viscosity of the EDL decreased exponentially with distance toward the bulk viscosity, consistent with the literature data.[39] For BmimCl solutions, η_D decreased more rapidly at the intermediate concentration ($c_s = 0.55$ M) than at the low ($c_s = 0.061$ M) and high ($c_s = 3.45$ M) concentrations. This reflects the fact that the screening length λ_D, represented as the dashed lines in Figure 6, exhibits a nonmonotonic dependence on c_s as described by eq 1. Similar behavior was observed for NaCl solutions.

CONCLUSIONS

In this work, we report the first detailed characterization of the viscoelasticity of the EDL in electrolyte solutions by measuring the resonant frequency and the energy dissipation of a quartz crystal oscillator for aqueous solutions containing three types of solutes: two electrolytes—an ionic liquid, 1-butyl-3-methylimidazolium chloride (BmimCl), and an ordinary salt, sodium chloride (NaCl)—and a nonelectrolyte, ethylene glycol (EG). The frequency and dissipation shifts for the nonelectrolyte EG solution are well predicted by the damping of the quartz oscillation in a Newtonian fluid, while excess frequency and dissipation shifts are observed over a wide ion concentration c_s range for the NaCl and BmimCl solutions. We attribute these excess shifts to the formation of an EDL on the quartz sensor crystal. The frequency shift due to the EDL decreases monotonically as c_s increases, while the dissipation shift due to the EDL increases monotonically as c_s increases. The complex shear modulus of the EDL is estimated by applying a wave propagation model in which the density and complex modulus of the EDL decay exponentially toward those of the bulk solution. The estimated storage and loss modulus of the EDL increase rapidly with increasing ion concentrations for $c_s < 1$ M but reach saturation values with similar magnitude at a sufficiently high ion concentration. This result suggests that the structure of the EDL near the charged surface becomes independent of the ion concentration. The shear viscosity near the charged QCM surface is approximately 50 times for NaCl solutions and 500 times for BmimCl solutions of the bulk solution value at the saturation concentration. This is consistent with the findings reported using the surface force apparatus.[39] Our study also demonstrates that a cost-effective, portable, and easy-to-use instrument such as QCM can be utilized for analyzing the rheological properties of the EDL in electrolyte solutions, thus providing a valid complementary alternative to conventional laboratory instruments such as the surface force apparatus.

ASSOCIATED CONTENT

Supporting Information

The Supporting Information is available free of charge at https://pubs.acs.org/doi/10.1021/acs.analchem.0c00475.

Longitudinal viscosity measurements, dielectric constant of aqueous solutions of BmimCl, ion diameter of BmimCl ions in water, atomic force microscopy, supporting figures, and table (PDF)

AUTHOR INFORMATION

Corresponding Author

Amy Q. Shen − *Micro/Bio/Nanofluidics Unit, Okinawa Institute of Science and Technology Graduate University, Okinawa 904-0495, Japan;* orcid.org/0000-0002-1222-6264; Email: amy.shen@oist.jp

Authors

Riccardo Funari − *Micro/Bio/Nanofluidics Unit, Okinawa Institute of Science and Technology Graduate University, Okinawa 904-0495, Japan;* orcid.org/0000-0003-1786-3833

Atsushi Matsumoto − *Micro/Bio/Nanofluidics Unit, Okinawa Institute of Science and Technology Graduate University, Okinawa 904-0495, Japan;* orcid.org/0000-0002-8157-3083

John R. de Bruyn − *Department of Physics and Astronomy, University of Western Ontario, London, Ontario N6A 3K7, Canada;* orcid.org/0000-0002-9431-6748

Complete contact information is available at: https://pubs.acs.org/10.1021/acs.analchem.0c00475

Author Contributions

R.F. and A.M. contributed equally.

Author Contributions

§R.F. and A.M. contributed equally.

Notes

The authors declare no competing financial interest.

https://dx.doi.org/10.1021/acs.analchem.0c00475
Anal. Chem. 2020, 92, 8244−8253

■ ACKNOWLEDGMENTS

The authors thank Sanyo Trading Co., Ltd. Japan, for the use of the acoustic spectrometer to measure the longitudinal viscosity, and Novaetech, Italy, for the energy dissipation analysis using their custom QCM software. The authors also thank Kang-Yu Chu from Micro/Bio/Nanofluidics Unit at OIST for his help with developing a MATLAB code for the data analysis. The authors acknowledge the support of the Okinawa Institute of Science and Technology Graduate University with subsidy funding from the Cabinet Office, Government of Japan. A.M. acknowledges funding from the Japanese Society for the Promotion of Science (Grants-in-Aid for Early-Career Scientists, Grant No. 19K15641). R.F. acknowledges funding from the Japanese Society for the Promotion of Science (Grants-in-Aid for Early-Career Scientists, Grant No. 20K20237). A.Q.S. acknowledges funding from the Japanese Society for the Promotion of Science (Grants-in-Aid for Scientific Research (C), Grant No. 17K06173 and Grants-in-Aid for Scientific Research (B), Grant No. 18H01135) and the Joint Research Projects (JRPs) supported by JSPS and SNSF. J.R.d.B. acknowledges funding from the Natural Sciences and Engineering Research Council of Canada.

■ REFERENCES

(1) Atkins, P. W.; De Paula, J.; Keeler, J. *Atkins' physical chemistry*; Oxford University Press: 2018.
(2) MacDonald, R.; Bangham, A. *J. Membr. Biol.* **1972**, *7*, 29−53.
(3) Guozhong, C. *Nanostructures and nanomaterials: synthesis, properties and applications*; World Scientific: 2004.
(4) Okubo, T. *Colloids Surf., A* **1996**, *109*, 77−88.
(5) Noh, C.; Jung, Y. *Phys. Chem. Chem. Phys.* **2019**, *21*, 6790−6800.
(6) Kim, S.; Kim, G. H.; Woo, H.; An, T.; Lim, G. *ACS Omega* **2020**, *5*, 3144−3150.
(7) Hossain, M. M.; Gurudatt, N. G.; Seo, K.-D.; Park, D.-S.; Hong, H.; Yeom, E.; Shim, J. H.; Shim, Y.-B. *Anal. Chem.* **2019**, *91*, 14109−14116.
(8) de Oliveira, R. A. G.; Nicoliche, C. Y. N.; Pasqualeti, A. M.; Shimizu, F. M.; Ribeiro, I. R.; Melendez, M. E.; Carvalho, A. L.; Gobbi, A. L.; Faria, R. C.; Lima, R. S. *Anal. Chem.* **2018**, *90*, 12377−12384.
(9) Tai, T.-Y.; Sinha, A.; Sarangadharan, I.; Pulikkathodi, A. K.; Wang, S.-L.; Lee, G.-Y.; Chyi, J.-I.; Shiesh, S.-C.; Lee, G.-B.; Wang, Y.-L. *Anal. Chem.* **2019**, *91*, 5953−5960.
(10) Taoka, M.; Horita, K.; Takekiyo, T.; Uekita, T.; Yoshimura, Y.; Ichimura, T. *Anal. Chem.* **2019**, *91*, 13494−13500.
(11) Roosen, C.; Müller, P.; Greiner, L. *Appl. Microbiol. Biotechnol.* **2008**, *81*, 607.
(12) Zhou, F.; Liang, Y.; Liu, W. *Chem. Soc. Rev.* **2009**, *38*, 2590−2599.
(13) Di Lecce, S.; Kornyshev, A. A.; Urbakh, M.; Bresme, F. *ACS Appl. Mater. Interfaces* **2020**, *12*, 4105−4113.
(14) Zhang, Y.; Cummings, P. T. *ACS Appl. Mater. Interfaces* **2019**, *11*, 42680−42689.
(15) Kitz, P. G.; Lacey, M. J.; Novàk, P.; Berg, E. J. *Anal. Chem.* **2019**, *91*, 2296−2303.
(16) Choi, Y.; Hwang, J.; Kim, K. M.; Jana, S.; Lee, S. U.; Chae, J.; Chang, J. *Anal. Chem.* **2019**, *91*, 5850−5857.
(17) Oldham, K. B. *J. Electroanal. Chem.* **2008**, *613*, 131−138.
(18) Etchenique, R.; Buhse, T. *Analyst* **2002**, *127*, 1347−1352.
(19) Armand, M.; Endres, F.; MacFarlane, D. R.; Ohno, H.; Scrosati, B. *Nat. Mater.* **2009**, *8*, 621−629.
(20) Atkin, R.; El Abedin, S. Z.; Hayes, R.; Gasparotto, L. H.; Borisenko, N.; Endres, F. *J. Phys. Chem. C* **2009**, *113*, 13266−13272.
(21) Perkin, S.; Albrecht, T.; Klein, J. *Phys. Chem. Chem. Phys.* **2010**, *12*, 1243−1247.
(22) Hayes, R.; Borisenko, N.; Tam, M. K.; Howlett, P. C.; Endres, F.; Atkin, R. *J. Phys. Chem. C* **2011**, *115*, 6855−6863.
(23) Perkin, S.; Crowhurst, L.; Niedermeyer, H.; Welton, T.; Smith, A. M.; Gosvami, N. N. *Chem. Commun.* **2011**, *47*, 6572−6574.
(24) Gebbie, M. A.; Valtiner, M.; Banquy, X.; Fox, E. T.; Henderson, W. A.; Israelachvili, J. N. *Proc. Natl. Acad. Sci. U. S. A.* **2013**, *110*, 9674−9679.
(25) Lee, A. A.; Vella, D.; Perkin, S.; Goriely, A. *J. Phys. Chem. Lett.* **2015**, *6*, 159−163.
(26) Cheng, H.-W.; Stock, P.; Moeremans, B.; Baimpos, T.; Banquy, X.; Renner, F. U.; Valtiner, M. *Adv. Mater. Interfaces* **2015**, *2*, 1500159.
(27) Gebbie, M. A.; Dobbs, H. A.; Valtiner, M.; Israelachvili, J. N. *Proc. Natl. Acad. Sci. U. S. A.* **2015**, *112*, 7432−7437.
(28) Black, J. M.; Zhu, M.; Zhang, P.; Unocic, R. R.; Guo, D.; Okatan, M. B.; Dai, S.; Cummings, P. T.; Kalinin, S. V.; Feng, G.; Balke, N. *Sci. Rep.* **2016**, *6*, 32389.
(29) Cui, T.; Lahiri, A.; Carstens, T.; Borisenko, N.; Pulletikurthi, G.; Kuhl, C.; Endres, F. *J. Phys. Chem. C* **2016**, *120*, 9341−9349.
(30) Smith, A. M.; Lee, A. A.; Perkin, S. *J. Phys. Chem. Lett.* **2016**, *7*, 2157−2163.
(31) Gavish, N.; Elad, D.; Yochelis, A. *J. Phys. Chem. Lett.* **2018**, *9*, 36−42.
(32) Gebbie, M. A.; Smith, A. M.; Dobbs, H. A.; Lee, A. A.; Warr, G. G.; Banquy, X.; Valtiner, M.; Rutland, M. W.; Israelachvili, J. N.; Perkin, S.; Atkin, R. *Chem. Commun.* **2017**, *53*, 1214−1224.
(33) Goodwin, Z. A.; Kornyshev, A. A. *Electrochem. Commun.* **2017**, *82*, 129−133.
(34) Lee, A. A.; Perez-Martinez, C. S.; Smith, A. M.; Perkin, S. *Faraday Discuss.* **2017**, *199*, 239−259.
(35) Smith, A. M.; Lee, A. A.; Perkin, S. *Phys. Rev. Lett.* **2017**, *118*, 096002.
(36) Coles, S. W.; Smith, A. M.; Fedorov, M. V.; Hausen, F.; Perkin, S. *Faraday Discuss.* **2018**, *206*, 427−442.
(37) Rotenberg, B.; Bernard, O.; Hansen, J.-P. *J. Phys.: Condens. Matter* **2018**, *30*, 054005.
(38) Gaddam, P.; Ducker, W. *Langmuir* **2019**, *35*, 5719−5727.
(39) Ueno, K.; Kasuya, M.; Watanabe, M.; Mizukami, M.; Kurihara, K. *Phys. Chem. Chem. Phys.* **2010**, *12*, 4066−4071.
(40) Kamijo, T.; Arafune, H.; Morinaga, T.; Honma, S.; Sato, T.; Hino, M.; Mizukami, M.; Kurihara, K. *Langmuir* **2015**, *31*, 13265−13270.
(41) Han, M.; Espinosa-Marzal, R. M. *ACS Appl. Mater. Interfaces* **2019**, *11*, 33465−33477.
(42) Sakuma, H.; Otsuki, K.; Kurihara, K. *Phys. Rev. Lett.* **2006**, *96*, 046104.
(43) Klein, J.; Kumacheva, E. *Science* **1995**, *269*, 816−819.
(44) Hellwig, J.; Micciulla, S.; Strebe, J.; von Klitzing, R. *Langmuir* **2016**, *32*, 10505−10512. PMID: 27610635.
(45) Monemian Esfahani, A.; Zhao, W.; Chen, J. Y.; Huang, C.; Xi, N.; Xi, J.; Yang, R. *Anal. Chem.* **2018**, *90*, 10340−10349. PMID: 30088414.
(46) Funari, R.; Della Ventura, B.; Schiavo, L.; Esposito, R.; Altucci, C.; Velotta, R. *Anal. Chem.* **2013**, *85*, 6392−6397.
(47) Funari, R.; Ripa, R.; Söderström, B.; Skoglund, U.; Shen, A. Q. *ACS sensors* **2019**, *4*, 3023−3033.
(48) Etchenique, R.; Buhse, T. *Analyst* **2000**, *125*, 785−787.
(49) Yoshimoto, M.; Tokimura, S.; Kurosawa, S. *Analyst* **2006**, *131*, 1175−1182.
(50) Encarnaçao, J. M.; Stallinga, P.; Ferreira, G. N. *Biosens. Bioelectron.* **2007**, *22*, 1351−1358.
(51) Granstaff, V. E.; Martin, S. J. *J. Appl. Phys.* **1994**, *75*, 1319−1329.
(52) Debye, P.; Huckel, E. *Z. Phys.* **1923**, *24*, 185.
(53) Endres, F.; Borisenko, N.; El Abedin, S. Z.; Hayes, R.; Atkin, R. *Faraday Discuss.* **2012**, *154*, 221−233.
(54) Cheng, H.-W.; Dienemann, J.-N.; Stock, P.; Merola, C.; Chen, Y.-J.; Valtiner, M. *Sci. Rep.* **2016**, *6*, 30058.

https://dx.doi.org/10.1021/acs.analchem.0c00475
Anal. Chem. 2020, 92, 8244−8253

(55) Amano, K.; Yokota, Y.; Ichii, T.; Yoshida, N.; Nishi, N.; Katakura, S.; Imanishi, A.; Fukui, K.; Sakka, T. *Phys. Chem. Chem. Phys.* **2017**, *19*, 30504−30512.
(56) Lee, A. A.; Perez-Martinez, C. S.; Smith, A. M.; Perkin, S. *Phys. Rev. Lett.* **2017**, *119*, 026002.
(57) Kjellander, R. *J. Chem. Phys.* **2018**, *148*, 193701.
(58) Ciach, A. *J. Mol. Liq.* **2018**, *270*, 138−144.
(59) Feng, G.; Chen, M.; Bi, S.; Goodwin, Z. A. H.; Postnikov, E. B.; Brilliantov, N.; Urbakh, M.; Kornyshev, A. A. *Phys. Rev. X* **2019**, *9*, 021024.
(60) Bazant, M. Z.; Storey, B. D.; Kornyshev, A. A. *Phys. Rev. Lett.* **2011**, *106*, 046102.
(61) Matsumoto, A.; Del Giudice, F.; Rotrattanadumrong, R.; Shen, A. Q. *Macromolecules* **2019**, *52*, 2759−2771.
(62) Voinova, M. V.; Rodahl, M.; Jonson, M.; Kasemo, B. *Phys. Scr.* **1999**, *59*, 391.
(63) Yang, F.; Wang, D.; Wang, X.; Liu, Z. *J. Chem. Eng. Data* **2017**, *62*, 3958−3966.
(64) Haynes, W. M. *CRC Handbook of Chemistry and Physics*; CRC Press: 2014.

https://dx.doi.org/10.1021/acs.analchem.0c00475
Anal. Chem. 2020, 92, 8244−8253